



REGULAR ARTICLE

Special Issue on THEORETICAL CHEMISTRY/CHEMICAL DYNAMICS

In silico studies of the early stages of aggregation of A β ₄₂ peptides[†]

PRABIR KHATUA and SANJOY BANDYOPADHYAY*

Molecular Modeling Laboratory, Department of Chemistry, Indian Institute of Technology, Kharagpur, West Bengal 721 302, India

E-mail: sanjoy@chem.iitkgp.ernet.in

MS received 26 December 2016; revised 3 February 2017; accepted 8 February 2017

Abstract. Accumulation of amyloid beta (A β) peptide in the brain is responsible for debilitating neurodegenerative disease, namely, Alzheimer's disease. We have carried out atomistic molecular dynamics simulation to study the early stages of the aggregation process of five full-length A β ₄₂ peptide monomers with varying secondary structural contents in aqueous solution. Attempts have been made to study the conformational modifications of the A β peptide monomers and their dynamical features during the oligomer formation. In particular, specific molecular interactions that drive the association process leading to the formation of the stable oligomer have been identified. The calculations revealed that the helix–helix linkage plays an important role for bringing the unstructured regions of the monomers closer for self-assembly. Importantly, it is demonstrated that the contribution originating from the nonpolar interactions between the peptides and the corresponding nonpolar solvation more than compensates the weakening effect of unfavorable inter-peptide electrostatic interactions, thereby stabilizing the nucleated oligomer.

Keywords. Molecular simulation; intrinsically disordered protein; amyloid β .

1. Introduction

Protein aggregation is closely linked with several neurodegenerative diseases, such as Alzheimer's disease, Parkinson's disease, Type II diabetes, Huntington's disease, etc.^{1,2} In general, such diseases are believed to be caused by the accumulation of β -sheet-rich structures termed as amyloid fibrils in the brain. Alzheimer's disease (AD) associated with the deposition of plaques or fibrils composed of 39 to 43 residue peptide named amyloid β -peptide (A β) in the brain is the most common form of dementia affecting millions of people worldwide. A β peptide is processed from sequential cleavage of the transmembrane amyloid precursor protein (APP) by β - and γ -secretases.³ The predominant components of fibrillar deposits in the brain of AD patients include A β peptides containing 40 and 42 amino acid residues (A β ₄₀ and A β ₄₂). Though A β ₄₂ peptide differs from A β ₄₀ by only two C-terminal residues, the former has a higher aggregation propensity as compared to the later.^{3,4}

A β ₄₂ monomer contains two hydrophobic patches, denoted as *hp1* (Leu-17 to Ala-21) and *hp2* (Ala-30 to Met-35) connected by a hydrophilic patch, denoted as *turn* (Glu-22 to Gly-29), the C-terminal

segment, denoted as *C-term* (Val-36 to Ala-42), and the disordered N-terminal segment (*N-term*) containing 16 residues (Asp-1 to Lys-16). A β fibril has U-shaped conformation with the β strands formed by the *hp1*, *hp2* and *C-term* segments.^{5,6} Importantly, the hydrophobic residues in *hp1* and *hp2* are believed to be primarily responsible for the hydrophobic collapse that occurs during fibrillation. In addition, the salt bridge formed between Asp-23 and Lys-28 in the hydrophilic *turn* region also plays a crucial role in bringing the *hp1* and *hp2* segments closer to form the β -hairpin structure, the basic unit of the fibril.^{7,8} The amino acid sequence of the A β ₄₂ peptide (in one letter code) is D(1)AEFRHDSGYEVVHQLVFFAEDVGSN-KGAILGLMVGGVVIA(42), with D(1) and A(42) being the N- and C-terminal residues, respectively.

A large body of literature exists on studying the self-assembly of A β from experiments as well as from theoretical and simulation studies. It is believed that amyloid formation follows a nucleation-dependent polymerization mechanism.^{9–11} According to this mechanism, fibril formation occurs in two phases, namely, the nucleation/lag phase and the elongation/growth phase. In nucleation phase, soluble monomers undergo conformational modifications and self-associate to form oligomeric nuclei. This process needs to overcome a high energy barrier and thus occurs slowly. In other

*For correspondence

[†]Dedicated to the memory of late Professor Charusita Chakravarty.

words, it is the rate limiting step of the amyloid formation. Nucleation phase is followed by thermodynamically favorable elongation/growth phase. Elongation phase, a faster process as compared to the nucleation phase is associated with the assembly of aggregates and fibril elongation. Neurotoxicity generated from the soluble oligomers and mature fibrils are thought to be the pathological reason for neuronal death of AD affected patients. Recently, it has been shown from several studies that soluble oligomers are more neurotoxic than the insoluble fibrils.^{12–15} Therefore, it is essential to characterize the soluble $A\beta$ oligomers and the mechanism of their formation from monomers in addition to studying the insoluble mature fibrils.

Establishing molecular details of the $A\beta$ aggregation and tracking the intermediate oligomeric structures along the aggregation pathways are two major challenging tasks in studying formation of amyloids. Structural informations of soluble $A\beta$ oligomers have been obtained from solid-state NMR studies.^{16,17} In these studies, small amounts of detergents or fatty acids were used to stabilize the soluble oligomers.^{16,17} For example, Yu et al.¹⁷ used sodium dodecyl sulphate (SDS) to make the soluble $A\beta$ oligomers long-lived and showed that such oligomers contain both parallel and anti-parallel β -sheet structures. X-ray crystallographic studies have also been performed to unravel the structures of soluble oligomers.^{18,19} However, such experimental techniques are often unable to precisely characterize the oligomers as they are highly prone to aggregation and often exist in diverse morphologies due to their inherent fluid-like character.²⁰ For example, x-ray crystallographic studies often yield data corresponding to the dominant conformational state. Ion-mobility mass spectrometry (IM-MS) is another important technique which can provide more accurate information as it is based on separating the oligomers according to their mass to charge ratio.^{21–23} Besides, IM-MS measures the collision cross-section which can be directly compared with the available experimental and theoretical findings. Recently, Kłoniecki *et al.*,²² detected two families of low-molecular-mass $A\beta_{40}$ oligomers, namely, compact and extended from IM-MS measurements.

Computer simulation can provide microscopic understanding of the interactions that drive the formation of $A\beta$ oligomers and the dynamics associated with the early events of fibril formation. Over the years, a number of simulation studies have been attempted to explore different aspects of this problem.^{24–31} In an important study, Urbanc *et al.*,²⁴ performed discrete molecular dynamics (DMD) simulations based on coarse-grained models to study in detail the dimer formations involving $A\beta_{40}$ and $A\beta_{42}$ peptides. The thermodynamic stability

of the dimer conformations as predicted by the DMD simulations were then examined using all-atom MD simulations. Based on the findings, they concluded that $A\beta$ oligomerization is not accompanied by the formation of thermodynamically stable planar β -strand dimers. A recent replica exchange molecular dynamics (REMD) study of $A\beta_{40}$ dimer showed that the β -hairpin peptide monomers formed by the central hydrophobic core region (*hp1* and *hp2*) prefer to arrange themselves in anti-parallel orientations in the dimeric form.²⁷

Most of the simulation studies reported in the literature are focused on probing the formation of lower order $A\beta$ oligomers, especially dimers. However, the lower order oligomers may not necessarily represent the characteristics of higher order $A\beta$ aggregates which eventually lead to the formation of protofibrils and fibrils.²⁹ Thus, it is essential to study higher order $A\beta$ oligomers for complete understanding of the driving forces behind $A\beta$ aggregation. In this study, we have performed MD simulation to characterize the early stages of formation of pentameric $A\beta$ aggregate starting from structurally different full-length $A\beta$ peptides in aqueous solution. Our primary objective has been to probe the conformational modifications of the $A\beta$ peptide monomers and their dynamical features during the early stages of the association process. Attempts have been made to identify specific molecular interactions that drive the self-assembly of the $A\beta$ peptide monomers leading to the formation of stable oligomers. In Section 2, we discuss the procedure followed to set up the system and the simulation protocols employed. The results obtained from the calculations are presented and discussed in Section 3. Finally, the important findings of the study and the conclusions reached therefrom are highlighted in Section 4.

2. System setup and simulation methods

We have used the NAMD code³² to carry out MD simulation of an aqueous solution containing five full-length $A\beta_{42}$ (henceforth will be simply denoted as $A\beta$) peptide monomers (designated as A1 to A5) with varying secondary structural contents to study the early stages of the aggregation process. The initial configuration of the monomer A1 was taken from model 5 of the solution state NMR structure (PDB ID: 1Z0Q).³³ We carried out 5 ns MD simulations at high temperatures of 450 K and 500 K with the A1 monomer to generate unstructured initial configurations corresponding to A2 and A3, respectively. The initial configurations of the $A\beta$ monomers A4 and A5 were obtained from replica exchange molecular dynamics (REMD) simulations³⁴ of the NMR structure with 64 replicas in the temperature range of 330 K to 600 K. Each replica was simulated for 10 ns with an

exchange time of 0.25 ps among the replicas and more than 10 % acceptance ratio. The last A β conformations as obtained from the trajectories at 530 K and 594 K were taken as the initial configurations of A4 and A5, respectively. It may be noted that the reason for considering A β monomers with different initial structures is due to the fact that A β being an intrinsically disordered protein (IDP) is highly flexible and exists in different conformational states in its monomeric form in aqueous environment. The terminal residues (Asp-1 and Ala-42) of each of the peptide monomers were taken as standard ammonium and carboxylate forms, respectively. After adding the hydrogen atoms, centers-of-mass of the peptide monomers were placed at least 20 Å away from each other in a cubic cell of dimension 85 Å containing appropriate number of equilibrated water molecules. To avoid unfavorable protein-water contacts, water molecules which were found within 2 Å of the peptide monomers were removed. 15 Na⁺ ions were then added to the system for charge neutralization.

The simulation system was first minimized using the conjugate-gradient energy minimization method as implemented in NAMD.³² The minimized initial configuration of the system is shown in Figure 1. For easy reference, the individual A β monomers are marked (A1 to A5) in the figure. The temperature of the system was then gradually increased to 310 K within a short MD run of 100 picoseconds (ps) under isothermal-isobaric ensemble (NPT) conditions at a constant pressure of 1 atm. The system was then equilibrated for 10 nanoseconds (ns) at 310 K under NPT ensemble conditions. The system temperature was controlled by using the Langevin dynamics method with a friction constant 1 ps⁻¹, whereas the

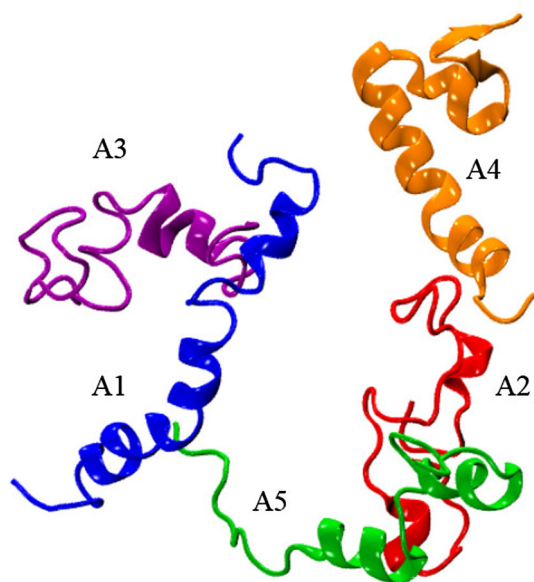


Figure 1. The initial configuration of the system containing the five A β monomers with varying secondary structural contents. For clarity, the peptide monomers designated as A1, A2, A3, A4, and A5 are shown in blue, red, purple, orange, and green colors, respectively.

pressure was controlled by the Nosé-Hoover Langevin piston method.³⁵ During this period, the simulation cell volume was allowed to fluctuate isotropically to attain the appropriate density. At this stage, the cell volume attained steady value with cell dimension 82.72 Å. The cell volume was then kept fixed and the simulation conditions were changed from constant pressure and temperature (NPT) to that of constant volume and temperature (NVT). The NVT equilibration run was then continued further at 310 K for another 5 ns, followed by a long NVT production run of 250 ns duration.

The simulation was carried out with an integration time step of 1 femtosecond (fs), and the trajectory was stored with a time resolution of 400 fs for subsequent analyses. The minimum image convention³⁶ was employed to calculate the short-range Lennard-Jones interactions using a spherical cut-off distance of 12 Å with a switch distance of 10 Å. The long-range electrostatic interactions were calculated by using the particle-mesh Ewald (PME) method.³⁷ All bonds involving the hydrogen atoms were constrained using the SHAKE algorithm³⁸. We have employed the all-atom CHARMM22 force field and potential parameters for the peptide,^{39,40} while the mTIP3P⁴¹ model (modified version of TIP3P⁴²) that is consistent with the chosen protein force field was employed for water.

3. Results and Discussion

3.1 Structural features

A few snapshots of the pentameric aggregate at different time intervals as obtained from our simulation are displayed in Figure 2. For easy reference, the initial configuration of the system containing the five A β peptide monomers is included in the figure. Conformational rearrangement of the monomers during their approach to form the oligomer is evident from the figure. It is noticed that such conformational rearrangement of the peptide monomers within the time scale of the simulation is associated with breaking and formation of secondary structural elements (helices, β -strands, turns/coils, etc.). Interestingly, an increase in helical content with time has been observed for a few monomers. This is particularly apparent for A2. Additionally, a closer look at the simulated trajectory reveals that the peptide monomers orient themselves in such a manner so that the helical segments of the adjacent monomers tend to associate with each other during the aggregation process. This is an important observation as close proximity of the helical segments of the monomers is likely to drive the oligomer formation by assisting the nucleation of the unstructured segments of the peptides adjacent to the helices. Our findings are consistent with experimental results where formation of helical intermediates that play important roles in the aggregation process has been suggested.^{43,44}

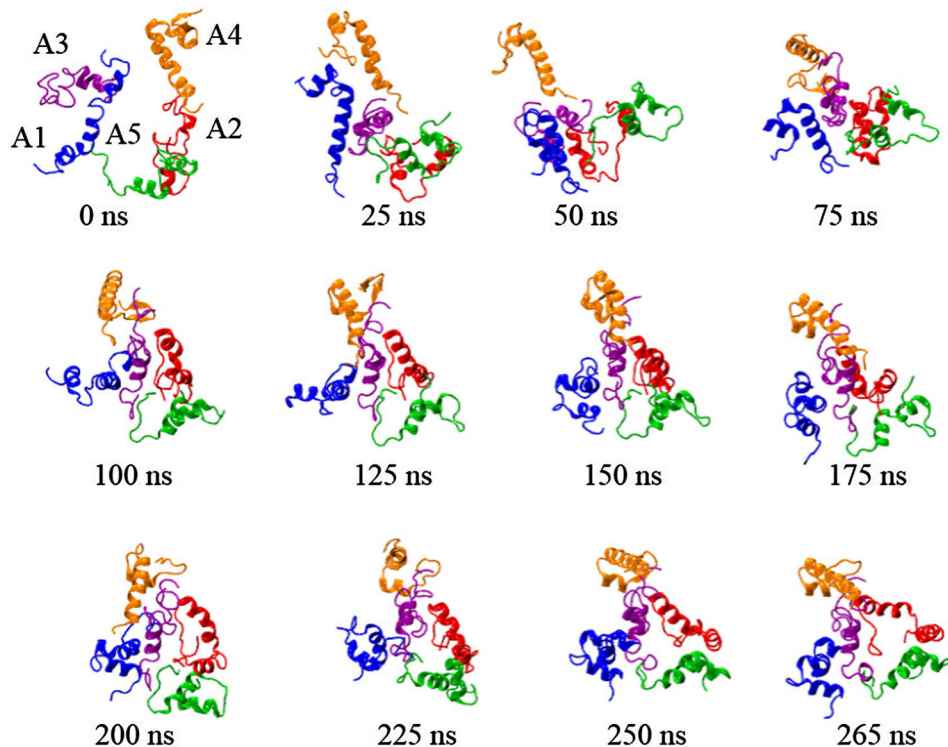


Figure 2. Snapshots of a few representative configurations of the simulated $A\beta$ pentameric aggregate at different time intervals. For clarity the initial configuration of the system is also included in the figure. The peptide coloring scheme is the same as that in Figure 1.

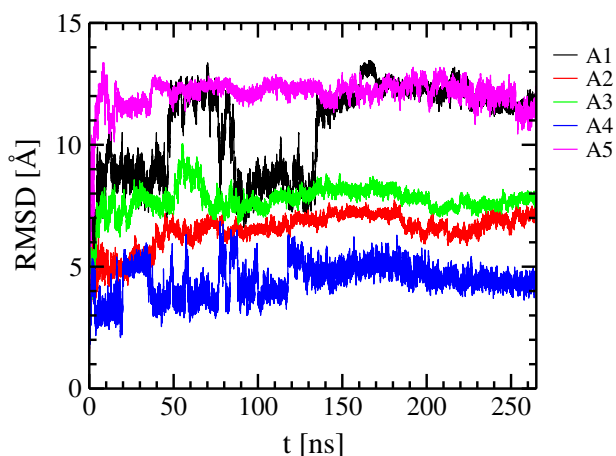


Figure 3. Time evolutions of RMSD corresponding to all the non-hydrogen atoms of the five $A\beta$ peptide monomers.

To investigate the flexibility of the $A\beta$ monomers and their conformational modifications during the nucleation process, we have monitored the root mean square deviations (RMSD) of the non-hydrogen atoms of each monomer independently. The results are depicted in Figure 3. It is clear from the figure that the peptide monomers deviate significantly from their initial structures. Besides, we observe several jumps in the RMSD

values, which suggests sharp conformational transitions of the peptides within the simulation time scale. We believe that such conformational changes of the monomers are key steps for their structural adaptations in the nucleated form. Interestingly, it may be noted that the RMSD of each of the monomers attains a steady limit within ~ 150 ns. This is an important finding as it provides an estimate of the time scale of structural adaptation necessary for the $A\beta$ peptides to form aggregated pentamer.

To quantify the aggregation of the $A\beta$ monomers, we have monitored the time evolution of the average center-of-mass distance between the closest pairs of the monomers (R_{CM}) during the simulation, as shown in Figure 4(a). As a reference, the initial value of R_{CM} (26.88 \AA) is marked in the figure (as straight line). Note the rapid decrease in the pairwise distance between the monomers within first 40 ns before attaining a steady mean value with minor fluctuations. This indicates formation of an aggregated pentameric form of the $A\beta$ peptide. The average R_{CM} value of $16.01 (\pm 0.32) \text{ \AA}$ as obtained over the last 100 ns of the simulated trajectory has been found to be $\sim 40\%$ lower than the corresponding initial value. The approach between the individual monomers during the aggregation process

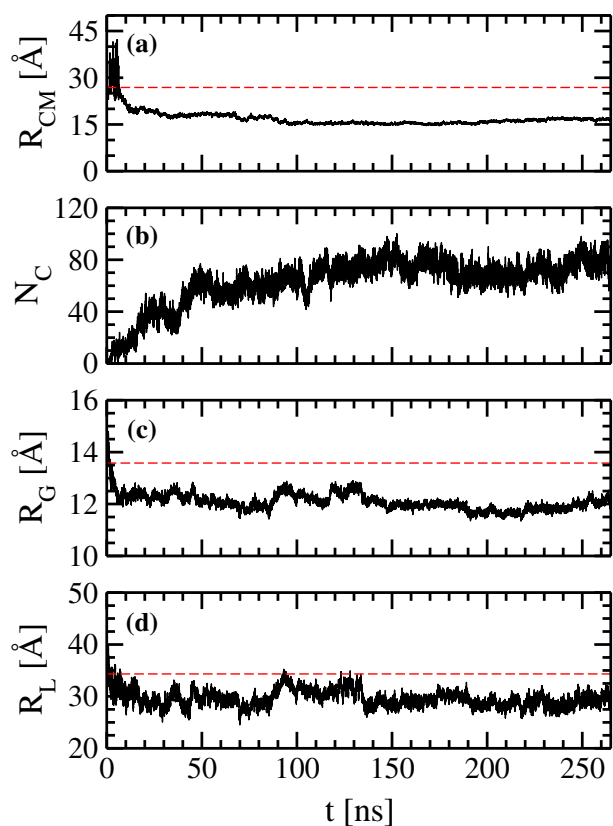


Figure 4. Time evolutions of (a) the average center-of-mass distance between two nearest monomers (R_{CM}), (b) the number of inter-peptide residue contact pairs (N_C), (c) the average radius of gyration (R_G) and (d) the average end-to-end distance (R_L) of the peptide monomers as obtained from the simulation.

should lead to the formation of pairwise inter-peptide residue contacts. The time evolution of the number of such contact pairs found between the A β monomers (N_C) is shown in Figure 4(b). We have considered two amino acid residues of two monomers to form a contact pair, if the distance between their C_α atoms is within 7 Å. An increase in the number of pairwise contacts with decreasing inter-peptide distance during the aggregation of the A β peptides is clearly evident from the data. In addition, it is important to probe the extent of structural adaptations undergone by the A β peptides while forming the aggregated oligomer. Radius of gyration (R_G) is an important physical parameter which can provide vital information on the size and shape fluctuations of the A β peptides during the nucleation process. We have shown the time evolution of R_G averaged over the A β monomers present in the pentameric system in Figure 4(c). As a reference, the initial average R_G value of 13.58 Å is marked in the figure by a straight line. It can be seen that the R_G value decreases sharply within first 10 ns and then tend to fluctuate around a mean value of 11.87 (\pm 0.09) Å over last 100 ns of the trajectory. A

decrease in R_G by \sim 13% with respect to the initial value indicates that the A β monomers undergo noticeable conformational transformations from expanded to compact forms during the association process. The time evolution of the peptide end-to-end distance (R_L) averaged over the A β monomers is shown in Figure 4(d). R_L is defined as the average distance between the C_α atoms of the two terminal residues of each of the peptide monomers. Again, the initial value of R_L (34.33 Å) is marked in the figure (as straight line) for comparison. Transformation of the A β monomers into compact forms during their self-assembly is once again evident from decreased R_L values with time. The calculated average R_L value of 29.04 (\pm 0.52) Å has been found to be \sim 15% lower than the initial value. Comparison of the results shown in Figure 4 clearly demonstrates that the nucleation of the A β monomers is associated with increased compactness and reduced distance between the end residues of the individual peptide monomers.

3.2 Secondary structure content

A closer examination of Figure 2 reveals change in secondary structural contents of the monomers during the aggregation process. In the previous section, we have discussed the possible role played by the helical segment of the peptide during aggregation. Here, we discuss the secondary structural contents of the peptide monomers in a more quantitative manner. For that, we have computed the residue-specific secondary structures of the monomers using the STRIDE algorithm⁴⁵ as implemented in the VMD tool.⁴⁶ The time evolutions of the secondary structures of the five A β monomers are displayed in Figure 5. The average secondary structural contents (in percentage) of the individual peptide monomers as obtained from the simulated trajectory along with the corresponding initial values are listed in Table 1. It is evident from the figure that in most cases, except A1, the residues present at the two ends of the peptide exhibit propensity to retain random coil-like conformations. Interestingly, we notice that the N-terminal end of A1 undergoes quasi-periodic transitions between coil and helical forms with noticeable lifetimes via momentary formation of β -strand like conformations. Residues Tyr-10 to Lys-16 in the *N-term* segment of A2 also exhibit such transitions within \sim 75 ns, before attaining a stable helical form for the rest of the trajectory. On the other hand, non-terminal residues present in the *N-term* and the two central hydrophobic segments *hp1* and *hp2* (Tyr-10 to Phe-20 and Ala-30 to Met-35) in general exhibit preference to either remain in helical form or transform from random coil to helical form. This is true for all the monomers

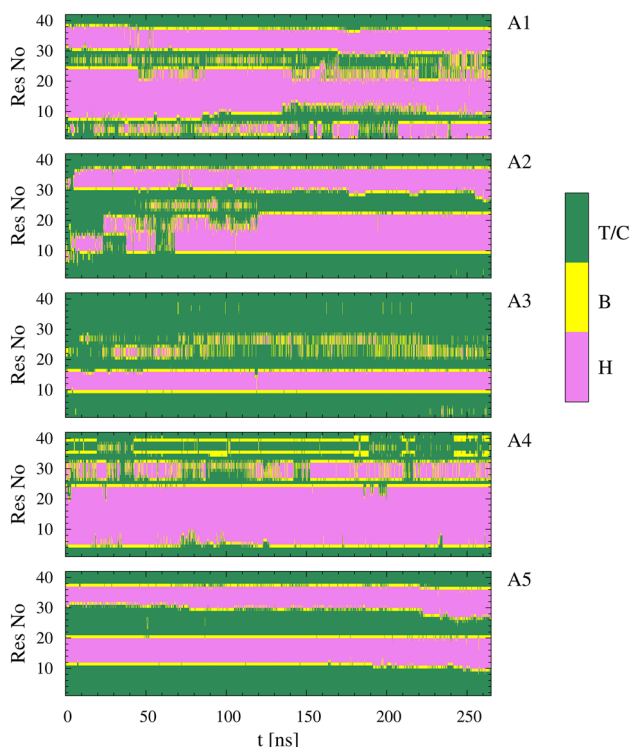


Figure 5. Time evolutions of residue-wise secondary structures of the five $A\beta$ peptide monomers as obtained from the simulation. The secondary structural elements, such as turn/coil (T/C), β -strand (B), and helix (H) are drawn in green, yellow, and magenta colors, respectively.

except the *hp2* segment of A3. Further, the figure shows that the central *turn* segment which was initially in random coil-like form in most cases, has shown noticeable tendency to interconvert into helical form. The data listed in Table 1 clearly show increased helical content of most of the monomers (except A4) associated with coil to helix transformations during the nucleation process. The influence on the β -content of the peptides has been found to be minimum. We believe that these are important findings that demonstrate that the formation of helical conformation in the hydrophobic core region of the peptide drives the early stages of the $A\beta$ aggregation process via the formation of helix-helix linkages among the monomers. To probe the secondary structural preference of the monomers present in the aggregated pentamer, in Figure 6 we show the average residue-wise secondary structural propensity. The calculation has been carried out over the last 100 ns of the equilibrated trajectory. It may be noted that during this time length, the monomers maintain steady separation distance between them with minimum conformational fluctuations (see Figures 3 and 4), indicating the formation of stable pentamer under the present conditions. It is observed that the residues present at the two ends

Table 1. The average secondary structural content (in percentage) of the five $A\beta$ peptide monomers.

monomer	helix	β -strand	turn/coil
A1	59.52 (50.00)	0.00 (0.00)	40.48 (50.00)
A2	43.78 (19.05)	1.45 (0.00)	54.77 (80.95)
A3	20.71 (16.67)	4.44 (0.00)	74.85 (83.33)
A4	56.69 (64.29)	7.96 (9.52)	35.34 (26.19)
A5	40.23 (38.10)	0.00 (0.00)	59.77 (61.90)

The values in the parentheses are the corresponding initial values.

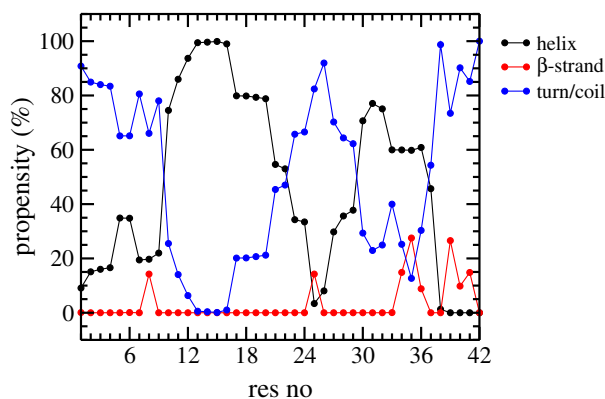


Figure 6. Average residue-wise secondary structural propensity (in %) of the $A\beta$ peptide monomers.

(Asp-1 to Gly-9 in *N-term* and Gly-38 to Ala-42 in *C-term*) and in the central *turn* region (Glu-22 to Gly-29) of the peptide exhibit propensity to be in random coil-like conformations. The random conformation of the *N-term* segment of the peptide as observed in this study is consistent with its experimentally known intrinsically disordered structure.⁵ Importantly, in consistent with Figure 5 one should note significantly higher propensity of the residues Tyr-10 to Phe-20 and Ala-30 to Met-35 forming the central hydrophobic core (*hp1* and *hp2*) to be in helical form.

3.3 Binding free energy

In this section, we calculate the binding free energy (ΔG_{bind}) of the aggregated $A\beta$ pentamer using the Molecular Mechanics Generalised Born Surface Area (MMGBSA) method,⁴⁷⁻⁵⁰ as implemented in AMBER14.^{51,52} According to the MMGBSA method,

ΔG_{bind} to form a complex can be written in general as⁴⁸

$$\Delta G_{bind} = \langle \Delta G_{MM} \rangle + \langle \Delta G_{sol} \rangle - T \langle \Delta S \rangle \quad (1)$$

where, ΔG_{MM} is the molecular mechanics contribution originating from the interactions between the ligand and the receptor, and ΔG_{sol} is the solvation free energy. $T \Delta S$ corresponds to the entropic contribution, which can be calculated either from the normal mode analysis⁵³ or using quasi-harmonic technique.⁵⁴ However, we have not included the entropy contribution arising from changes in the degrees of freedom (translational, rotational, and vibrational) in our calculation due to its high computational demand. Thus, the binding free energy reported in our calculation is indeed the sum of ΔG_{MM} and ΔG_{sol} ,⁵⁵ i.e.,

$$\Delta G_{bind} = \langle \Delta G_{MM} \rangle + \langle \Delta G_{sol} \rangle \quad (2)$$

ΔG_{MM} is the sum of the contributions originating from the inter-molecular electrostatic and van der Waals (vdw) interaction terms (ΔG_{elec} and ΔG_{vdw}), and can be written as

$$\Delta G_{MM} = \Delta G_{elec} + \Delta G_{vdw} \quad (3)$$

We have calculated ΔG_{elec} and ΔG_{vdw} using the SANDER module of AMBER.^{51,52} The total solvation free energy (ΔG_{sol}) has also been divided into electrostatic and nonpolar components (ΔG_{GB}) and ΔG_{nps}) as

$$\Delta G_{sol} = \Delta G_{GB} + \Delta G_{nps} \quad (4)$$

The electrostatic solvation free energy, ΔG_{GB} , has been calculated using the generalised Born (GB) method.⁵⁶ On the other hand, the nonpolar contribution to the solvation free energy (ΔG_{nps}) has been calculated as a function of the solvent accessible surface area (SASA), given as^{57,58}

$$\Delta G_{nps} = \gamma \times SASA + b \quad (5)$$

where, the constants γ and b were set to 0.005 kcal mol⁻¹ Å⁻² and 0.0, respectively.⁵¹ Following the discussion, we can rewrite equation 2 for the total binding free energy as

$$\Delta G_{bind} = \langle \Delta G_{nonpolar} \rangle + \langle \Delta G_{GB,elec} \rangle \quad (6)$$

Here $\Delta G_{nonpolar}$ and $\Delta G_{GB,elec}$ correspond to the contributions originating from non-polar and electrostatic interactions, respectively, which are given by

$$\Delta G_{nonpolar} = \Delta G_{vdw} + \Delta G_{nps} \quad (7)$$

and

$$\Delta G_{GB,elec} = \Delta G_{GB} + \Delta G_{elec} \quad (8)$$

The average binding free energy (ΔG_{bind}) and the corresponding components for the whole peptide monomer

in the nucleated pentameric form as obtained from the last 100 ns of the simulation are listed in Table 2. At first, negative ΔG_{bind} value of -50 kcal mol⁻¹ for the whole peptide suggests that the nucleation of the Aβ monomers to form the pentameric aggregate is thermodynamically favorable. However, a closer look at the contributions originating from different interactions in ΔG_{bind} reveal interesting behavior. It can be seen that while the nonpolar contribution ($\Delta G_{nonpolar}$) to the binding free energy is favorable, opposite is the case for the electrostatic component ($\Delta G_{GB,elec}$). Further, we notice that though both van der Waals component involving the peptide monomers (ΔG_{vdw}) and their nonpolar solvation (ΔG_{nps}) make favorable contributions, but the former contributes $\sim 85\%$ of $\Delta G_{nonpolar}$. Interestingly, the contributions originating from electrostatic interactions provide a contrasting picture. It is found that while the polar solvation term (ΔG_{GB}) of the peptides favors the nucleation process, but the unfavorable inter-peptide electrostatic interaction more than compensates the effect of solvation. Such counter-play between the two components weakens the overall electrostatic contribution, thereby resulting in a destabilizing influence on the nucleation process of the Aβ peptide monomers.

We have also calculated the free energy contributions of different secondary structural segments of the Aβ peptide (averaged over the last 100 ns of the trajectory) toward forming the aggregate, which are listed in Table 2. It is apparent that except *C-term*, other segments of the peptide contribute favorably to the binding free energy (ΔG_{bind}). In particular, the core hydrophobic segments *hp1* and *hp2* contribute maximum toward negative ΔG_{bind} value. This suggests that the favorable binding between the Aβ peptide monomers during the aggregation process proceeds via preferential association of the hydrophobic segments, *hp1* and *hp2*. On the other hand, the positive value of ΔG_{bind} for the *C-term* segment suggests that it is unlikely to remain bound in the aggregated state. Importantly, the calculation reveals that the unfavorable contribution of $\Delta G_{GB,elec}$ primarily originate from repulsive electrostatic interactions (ΔG_{elec}) involving the two terminal segments of the peptide (*N-term* and *C-term*) which are not adequately compensated by the polar component of the solvation free energy, ΔG_{GB} .

It is clear from the above discussion that except the *C-term* segment, association between the other segments of the Aβ peptide monomers during the early stages of the aggregation process is thermodynamically favorable. Now, it would be interesting to probe the residue-wise contributions to the binding free energy of the peptides. For that, we have calculated the

Table 2. Binding free energies and the corresponding components (in kcal mol⁻¹) for different segments of the A β peptide in the nucleated pentameric form as obtained using the MMGBSA method.

segment	ΔG_{vdw}	ΔG_{elec}	ΔG_{GB}	ΔG_{nps}	$\Delta G_{nonpolar}$	$\Delta G_{GB,elec}$	ΔG_{bind}
Whole	-133.92	296.08	-189.70	-22.52	-156.44	106.38	-50.06
N-term	-47.09	48.62	-0.58	-9.30	-56.39	48.04	-8.35
hp1	-21.64	-12.76	20.84	-3.71	-25.35	8.08	-17.27
Turn	-12.85	78.47	-70.06	-2.47	-15.32	8.41	-6.91
hp2	-36.27	-6.27	16.31	-5.78	-42.05	10.04	-32.01
C-term	-16.07	188.03	-156.21	-4.92	-20.99	31.82	10.83

The corresponding values averaged over the whole peptide monomers are also listed.

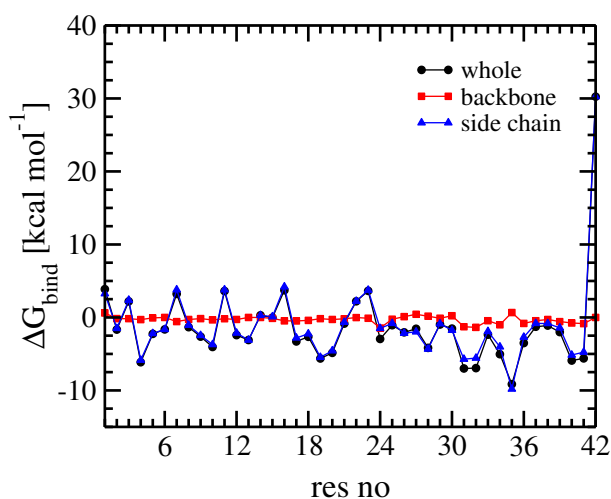


Figure 7. Average residue-wise binding free energy of the A β peptide monomers. The contributions originating from the backbones and the side chains of the residues are also shown.

ΔG_{bind} value for each of the amino acid residues averaged over all the peptide monomers and over the last 100 ns of the trajectory. The results are displayed in Figure 7. We have also decomposed the total binding free energy into the contributions originating from the backbones and the side chains of the residues, as shown in the figure. It is found that the contribution from the residue backbones is almost zero. This indicates that the interactions between the residue side chains play dominant role in controlling the formation and stability of the aggregated form. Importantly, we notice that besides the two terminal residues, most of the other residues that contribute unfavorably to ΔG_{bind} , namely, Glu-3, Asp-7, Glu-11, Lys-16, Glu-22, Asp-23, contain long side chains that are charged. On the other hand, most of the other residues that make favorable contribution to ΔG_{bind} are either non-polar or polar uncharged residues. This provides microscopic justification of our earlier finding between the contrasting contributions of electrostatic and non-polar interactions toward the overall

binding free energy of the aggregate. Note that most of the residues with unfavorable free energy contributions are negatively charged. This is an important observation, which suggests that the side chains of these residues are required to orient in such a manner so that the overall electrostatic repulsion between them minimizes, thereby resulting in formation of stable A β peptide aggregates. We are currently exploring this aspect in greater detail in our laboratory.

4. Conclusions

In this article, we have carried out atomistic MD simulation to study the early stages of the aggregation process of A β peptides in aqueous environment. Efforts have been made to obtain a microscopic understanding of the conformational modifications of the peptide monomers that occur during the nucleation process and the thermodynamic origin behind that.

The calculations revealed breaking and formation of secondary structural elements with a relative increase in helical content for most of the peptide monomers within the time scale of the simulation. Importantly, it is found that the peptide monomers tend to orient themselves in such a manner so that the helical segments of the adjacent monomers associate with each other during the aggregation process. Propensity to form helical structures by A β peptides is consistent with experimental observations at an early aggregation stage.^{43,44} It is further demonstrated that the structural adaptations of the A β monomers during nucleation is associated with their increased compactness.

The binding free energy of the nucleated A β pentamer as obtained from our calculations revealed that the early stages of the aggregation process involving A β peptides are thermodynamically favorable. Importantly, it is observed that the contribution originating from nonpolar van der Waals interactions between the peptides and the corresponding nonpolar solvation more

than compensates the weakening effect of unfavorable inter-peptide electrostatic interactions, thereby stabilizing the nucleated oligomer. It is further shown that the favorable binding between the A β peptide monomers during the aggregation process proceeds via preferential association of the hydrophobic segments, *hp1* and *hp2*. We believe that the long side chains of the charged peptide residues need to orient appropriately during their approach toward each other so that the overall electrostatic repulsion between them is minimized to form thermodynamically stable A β aggregates.

Acknowledgements

This study was supported by grants from the Department of Science and Technology (DST), Government of India, under the DST-FIST programme and the DST-IYC award. PK thanks University Grants Commission (UGC), Government of India for providing a scholarship. We thank Dr. Neelanjana Sengupta for many useful discussions.

References

1. Uversky V N, Oldfield C J and Dunker A K 2008 Intrinsically Disordered Proteins in Human Diseases: Introducing the D² Concept *Annu. Rev. Biophys.* **37** 215
2. Chiti F and Dobson C M 2006 Protein Misfolding, Functional Amyloid, and Human Disease *Annu. Rev. Biochem.* **75** 333
3. Haass C and Selkoe D J 2007 Soluble Protein Oligomers in Neurodegeneration: Lessons from the Alzheimer's Amyloid β -Peptide *Nat. Rev. Mol. Cell Biol.* **8** 101
4. Riek R, Güntert P, Döbeli H, Wipf B and Wüthrich K 2001 NMR Studies in Aqueous Solution Fail to Identify Significant Conformational Differences Between the Monomeric Forms of Two Alzheimer Peptides with Widely Different Plaque-Competence, A β (1–40) ox and A β (1–42) ox *Eur. J. Biochem.* **268** 5930
5. Lührs T, Ritter C, Adrian M, Riek-Loher D, Bohrmann B, Döbeli H, Schubert D and Riek R 2005 3D Structure of Alzheimer's Amyloid- β (1–42) Fibrils *Proc. Natl. Acad. Sci. USA* **102** 17342
6. Tycko R 2004 Progress Towards a Molecular-Level Structural Understanding of Amyloid Fibrils *Curr. Opin. Struct. Biol.* **14** 96
7. Petkova A T, Ishii Y, Balbach J J, Antzutkin O N, Leapman R D, Delaglio F and Tycko R 2002 A Structural Model for Alzheimer's β -Amyloid Fibrils Based on Experimental Constraints from Solid State NMR *Proc. Natl. Acad. Sci. USA* **99** 16742
8. Han W and Wu Y-D 2005 A Strand-Loop-Strand Structure is a Possible Intermediate in Fibril Elongation: Long Time Simulations of Amyloid- β Peptide (10–35) *J. Am. Chem. Soc.* **127** 15408
9. Jarrett J T and Lansbury Jr P T 1993 The Carboxy Terminus of the Beta Amyloid Protein is Critical for the Seeding of Amyloid Formation: Implications for the Pathogenesis of Alzheimer's Disease *Cell* **73** 1055
10. Harper J D and Lansbury Jr P T 1997 Models of Amyloid Seeding in Alzheimer's Disease and Scrapie: Mechanistic Truths and Physiological Consequences of the Time-Dependent Solubility of Amyloid Proteins *Annu. Rev. Biochem.* **66** 385
11. Naiki H and Gejyo F 1999 [20] Kinetic Analysis of Amyloid Fibril Formation *Methods Enzymol.* **309** 305
12. Kaye R, Head E, Thompson J L, McIntire T M, Milton S C, Cotman C W and Glabe C G 2003 Common Structure of Soluble Amyloid Oligomers Implies Common Mechanism of Pathogenesis *Science* **300** 486
13. Kaye R, Sokolov Y, Edmonds B, McIntire T M, Milton S C, Hall J E and Glabe C G 2004 Permeabilization of Lipid Bilayers is a Common Conformation-Dependent Activity of Soluble Amyloid Oligomers in Protein Misfolding Diseases *J. Biol. Chem.* **279** 46363
14. Lesné S, Koh M T, Kotilinek L, Kaye R, Glabe C G, Yang A, Gallagher M and Ashe K H 2006 A Specific Amyloid- β Protein Assembly in the Brain Impairs Memory *Nature* **440** 352
15. Wasling P, Daborg J, Riebe I, Andersson M, Portelius E, Blennow K, Hanse E and Zetterberg H 2009 Synaptic Retrogenesis and Amyloid- β in Alzheimer's Disease *J. Alzheimer's Dis.* **16** 1
16. Rangachari B D, Reed D K, Sonoda L K, Bridges A W, Conboy E, Hartigan D and Rosenberry T L 2007 Amyloid- β (1–42) Rapidly Forms Protofibrils and Oligomers by Distinct Pathways in Low Concentrations of Sodium Dodecylsulfate *Biochemistry* **46** 12451
17. Yu L, Edalji R, Harlan J E, Holzman T F, Lopez A P, Labkovsky B, Hillen H, Barghorn S, Ebert U, Richardson P L, Miebauer L, Solomon L, Bartley D, Walter K, Johnson R W, Hajduk P J and Olejniczak E T 2009 Structural Characterization of a Soluble Amyloid β -Peptide Oligomer *Biochemistry* **48** 1870
18. Pham J D, Chim N, Goulding C W and Nowick J S 2013 Structures of Oligomers of a Peptide from β -Amyloid *J. Am. Chem. Soc.* **135** 12460
19. Spencer R K, Li H and Nowick J S 2014 X-Ray Crystallographic Structures of Trimers and Higher-Order Oligomeric Assemblies of a Peptide Derived from A β _{17–36} *J. Am. Chem. Soc.* **136** 5595
20. Ahmed M, Davis J, Aucoin D, Sato T, Ahuja S, Aimoto S, Elliott J I, Van Nostrand W E and Smith S O 2010 Structural Conversion of Neurotoxic Amyloid-[Beta] 1–42 Oligomers to Fibrils *Nat. Struct. Mol. Biol.* **17** 561
21. Jablonowska A, Bakun M, Kupniewska-Kozak A and Dadlez M 2004 Alzheimer's Disease A β Peptide Fragment 10–30 forms a Spectrum of Metastable Oligomers with Marked Preference for N to N and C to C Monomer Termini Proximity *J. Mol. Biol.* **344** 1037
22. Kłoniecki M, Jablonowska A, Poznański J, Langridge J, Hughes C, Campuzano I, Giles K and Dadlez M 2011 Ion Mobility Separation Coupled with MS Detects Two Structural States of Alzheimer's Disease A β _{1–40} Peptide Oligomers *J. Mol. Biol.* **407** 110
23. Do T D, LaPointe N E, Nelson R, Krotee P, Hayden E Y, Ulrich B, Quan S, Feinstein S C, Teplow D B, Eisenberg D, Shea J-E and Bowers M T 2016 Amyloid β -Protein C-Terminal Fragments: Formation of Cylindrins and β -Barrels *J. Am. Chem. Soc.* **138** 549

24. Urbanc B, Cruz L, Ding F, Sammond D, Khare S, Buldyrev S V, Stanley H E and Dokholy N V 2004 Molecular Dynamics Simulation of Amyloid β Dimer Formation *Biophys. J.* **87** 2310
25. Jang S and Shin S 2006 Amyloid β -Peptide Oligomerization in Silico: Dimer and Trimer *J. Phys. Chem. B* **110** 1955
26. García A E, Gnanakaran S and Nussinov R 2006 Atomic-Level Description of Amyloid β -Dimer Formation *J. Am. Chem. Soc.* **128** 2158
27. Côté S, Laghaei R, Derreumaux P and Mousseau N 2012 Distinct Dimerization for Various Alloforms of the Amyloid-Beta Protein: $A\beta$ 1-40, $A\beta$ 1-42, and $A\beta$ 1-40 (D23N) *J. Phys. Chem. B* **116** 4043
28. Tarus B, Tran T T, Nasica-Labouze J, Sterpone F, Nguyen P H and Derreumaux P 2015 Structures of the Alzheimers Wild-Type $A\beta$ 1-40 Dimer from Atomistic Simulations *J. Phys. Chem. B* **119** 10478
29. Nguyen P H, Li M S, Stock G, Straub J E and Thirumalai D 2007 Monomer Adds to Preformed Structured Oligomers of $A\beta$ -Peptides by a Two-Stage Dock-Lock Mechanism *Proc. Natl. Acad. Sci. USA* **104** 111
30. Kim S, Takeda T and Klimov D K 2010 Mapping Conformational Ensembles of $A\beta$ Oligomers in Molecular Dynamics Simulations *Biophys. J.* **99** 1949
31. Urbanc B, Betnel M, Cruz L, Bitan G and Teplow D B 2010 Elucidation of Amyloid β -Protein Oligomerization Mechanisms: Discrete Molecular Dynamics Study *J. Am. Chem. Soc.* **132** 4266
32. Phillips J C, Braun R, Wang W, Gumbart J, Tajkhorshid E, Villa E, Chipot C, Skeel R D, Kale L and Schulten K 2005 Scalable Molecular Dynamics with NAMD *J. Comput. Chem.* **26** 1781
33. Tomaselli S, Esposito V, Vangone P, van Nuland N A J, Bonvin A M J J, Guerrini R, Tancredi T, Temussi P A and Picone D 2006 The α -to- β Conformational Transition of Alzheimer's $A\beta$ -(1-42) Peptide in Aqueous Media is Reversible: A Step by Step Conformational Analysis Suggests the Location of β Conformation Seeding *ChemBioChem* **7** 257
34. Sugita Y and Okamoto Y 1999 Replica-Exchange Molecular Dynamics Method for Protein Folding *Chem. Phys. Lett.* **314** 141
35. Feller S E, Zhang Y, Pastor R W and Brooks B R 1995 Constant Pressure Molecular Dynamics Simulation: The Langevin Piston Method *J. Chem. Phys.* **103** 4613
36. Allen M P and Tildesley D J 1987 In *Computer Simulation of Liquids* (Oxford: Oxford University Press)
37. Darden T, York, D and Pedersen L 1993 Particle Mesh Ewald: An $N \log(N)$ Method for Ewald Sums in Large Systems *J. Chem. Phys.* **98** 10089
38. Ryckaert J-P, Ciccotti G and Berendsen H J C 1977 Numerical Integration of the Cartesian Equations of Motion of a System with Constraints: Molecular Dynamics of n-Alkanes *J. Comput. Phys.* **23** 327
39. MacKerell A D, Bashford D, Bellott M L D R, Dunbrack R L, Evanseck J D, Field M J, Fischer S, Gao J, Guo H, Ha S, Joseph-McCarthy D, Kuchnir L, Kuczera K, Lau F T K, Mattos C, Michnick S, Ngo T, Nguyen D T, Prodhom B, Reiher W E, Roux B, Schlenkrich M, Smith J C, Stote R, Straub J, Watanabe M, Wiórkiewicz-Kuczera J, Yin D and Karplus M 1998 All-Atom Empirical Potential for Molecular Modeling and Dynamics Studies of Proteins *J. Phys. Chem. B* **102** 3586
40. MacKerell A D, Feig M and Brooks C L 2004 Extending the Treatment of Backbone Energetics in Protein Force Fields: Limitations of Gas-Phase Quantum Mechanics in Reproducing Protein Conformational Distributions in Molecular Dynamics Simulations *J. Comput. Chem.* **25** 1400
41. Neria E, Fischer S and Karplus M 1996 Simulation of Activation Free Energies in Molecular Systems *J. Chem. Phys.* **105** 1902
42. Jorgensen W L, Chandrasekhar J, Madura J D, Impey R W and Klein M L 1983 Comparison of Simple Potential Functions for Simulating Liquid Water *J. Chem. Phys.* **79** 926
43. Abedini A and Raleigh D P 2009 A Role for Helical Intermediates in Amyloid Formation by Natively Unfolded Polypeptides? *Phys. Biol.* **6** 015005
44. Abedini A and Raleigh D P 2009 A Critical Assessment of the Role of Helical Intermediates in Amyloid Formation by Natively Unfolded Proteins and Polypeptides *Protein Eng. Des. Sel.* **22** 453
45. Frishman D and Argos P 1995 Knowledge-Based Protein Secondary Structure Assignment *Proteins* **23** 566
46. Humphrey W, Dalke A, Schulten K 1996 VMD: Visual Molecular Dynamics *J. Mol. Graphics* **14** 33
47. Srinivasan J, Cheatham III T E, Cieplak P, Kollman P A and Case D A 1998 Continuum Solvent Studies of the Stability of DNA, RNA, and Phosphoramidate-DNA Helices *J. Am. Chem. Soc.* **120** 9401
48. Kollman P A, Massova I, Reyes C, Kuhn B, Huo S, Chong L, Lee M, Lee T, Duan Y, Wang W, Donini O, Cieplak P, Srinivasan J, Case D A and Cheatham III T E 2000 Calculating Structures and Free Energies of Complex Molecules: Combining Molecular Mechanics and Continuum Models *Acc. Chem. Res.* **33** 889
49. Deng N-J and Cieplak P 2009 Insights into Affinity and Specificity in the Complexes of α -Lytic Protease and Its Inhibitor Proteins: Binding Free Energy from Molecular Dynamics Simulation *Phys. Chem. Chem. Phys.* **11** 4968
50. Hou T, Wang J, Li Y and Wang W 2010 Assessing the Performance of the MM/PBSA and MM/GBSA Methods. 1. The Accuracy of Binding Free Energy Calculations Based on Molecular Dynamics Simulations *J. Chem. Inf. Model* **51** 69
51. Case D A, Babin V, Berryman J, Betz R M, Cai Q, Cerutti D S, Cheatham III T E, Darden T A, Duke R E, Gohlke H, Goetz A W, Gusarov S, Homeyer N, Janowski P, Kaus J, Kolossv'ary I, Kovalenko A, Lee T S, LeGrand S, Luchko T, Luo R, Madej B, Merz K M, Paesani F, Roe D R, Roitberg A, Sagui C, Salomon-Ferrer R, Seabra G, Simmerling C L, Smith W, Swails J, Walker R C, Wang J, Wolf R M, Wu X and Kollman P A 2014 Amber 14
52. Miller III B R, McGee Jr T D, Swails J M, Homeyer N, Gohlke H and Roitberg A E 2014 MMPBSA.py: An Efficient Program for End-State Free Energy Calculations *J. Chem. Theory. Comput.* **8** 3314
53. McQuarrie D A 2000 In *Statistical Mechanics* 2nd edn. (Herndon: University Science Books)
54. Brooks B R, Janežič D and Karplus M 1995 Harmonic Analysis of Large Systems. I. Methodology *J. Comput. Chem.* **16** 1522

55. Liu F F, Liu Z, Bai S, Dong X Y and Sun Y 2012 Exploring the Inter-Molecular Interactions in Amyloid β Protofibril with Molecular Dynamics Simulations and Molecular Mechanics Poisson–Boltzmann Surface Area Free Energy Calculations *J. Chem. Phys.* **136** 145101
56. Onufriev A, Bashford D and Case D A 2004 Exploring protein native states and large-scale conformational changes with a modified generalized Born model *Proteins* **55** 383
57. Hermann R B 1972 Theory of hydrophobic bonding. II. correlation of hydrocarbon solubility in water with solvent cavity surface area *J. Phys. Chem.* **76** 2754
58. Amidon G L, Yalkowsky S H, Anik S T and Valvani S C 1975 Solubility of Nonelectrolytes in Polar Solvents. V. Estimation of the Solubility of Aliphatic Monofunctional Compounds in Water Using a Molecular Surface Area Approach *J. Phys. Chem.* **79** 2239